Materials Horizons

COMMUNICATION

View Article Online
View Journal | View Issue

Cite this: *Mater. Horiz.*, 2019, 6, 587

Received 10th July 2018,
Accepted 5th November 2018

DOI: 10.1039/c8mh00809d

rsc.li/materials-horizons

MoS_2-capped Cu_xS nanocrystals: a new heterostructured geometry of transition metal dichalcogenides for broadband optoelectronics†

Yuan Li, [abc] Akshay A. Murthy,[be] Jennifer G. DiStefano,[b] Hee Joon Jung, [bc] Shiqiang Hao,[b] Cesar J. Villa,[b] Chris Wolverton,[b] Xinqi Chen*[cd] and Vinayak P. Dravid *[bce]

Heterostructuring of different transition metal dichalcogenides (TMDs) leads to interesting band alignment and performance improvement, and thus enables new routes for the development of materials for next-generation semiconductor electronics. Herein, we introduce a new strategy for the design and synthesis of functional TMD heterostructures. The representative product, molybdenum disulfide-capped copper sulfide (Cu_xS@MoS_2, $1.8 < x < 2.0$), is typically obtained by chemical vapor deposition of cap-like MoS_2 layers on Cu_xS nanocrystals, yielding the formation of a sharp, clean heterojunction interface. The heterostructures exhibit strong light–matter interactions over a broadband range, with interesting band alignment for separating photocarriers and mediating charge transfer. A phototransistor made from Cu_xS@MoS_2 heterostructures shows particularly high photoresponse for near infrared light, which is enabled by the heterojunction of MoS_2 with a small band gap semiconductor as well as the plasmonic enhancement from the Cu_xS nanocrystals. Our study paves a way for the development of new TMD heterostructures towards achieving functional electronics and optoelectronics.

Conceptual insights

Conventional TMD heterostructures, aligned in lateral or vertical geometries (*e.g.*, MoS_2/WS_2, $MoSe_2$/WSe_2, WSe_2/MoS_2, *etc.*), exhibit new chemical, structural and electronic properties for various applications in transistors, diodes and photovoltaic/photodetection devices. However, the main protocols, mechanical transfer and chemical vapor deposition, for preparing such heterostructures, are limited by their inevitable interface contamination and lack of massive and constant yields. Beyond the scope of such traditional heterostructures, our study reports a critical scientific step forward for bringing the concept of a new heterostructural geometry (namely MoS_2-capped Cu_xS nanocrystals) into the family of TMD heterostructures. Using a direct chemical vapor deposition approach, we are able to create an atomically clean interface between the Cu_xS core and MoS_2 cap, which, as compared with conventional TMD heterostructures, effectively maximized the interfacial area and would be very facile to realize large-scale production. Our structural design and synthesis strategy of the MoS_2-capped Cu_xS nanocrystals can be generalized to abundant TMD materials and thus allow for a wide range of explorations across diverse disciplines and the originality of the approach.

1. Introduction

Semiconductor heterostructures are essential components in modern high-speed electronics and optoelectronic devices.[1] With the need for continued device scaling to achieve faster and miniaturized electronic components, new semiconductor systems such as two-dimensional (2D) transition metal dichalcogenides (TMDs) have attracted wide attention due to their unique layer-dependent electronic and optical properties.[2–4] When these TMD semiconductors are combined in tandem, exciting new chemical, structural and electronic properties for various applications, such as transistors, diodes and photovoltaic/photodetection devices, are observed.[5–10] For instance, heterostructures of layered TMDs (*e.g.*, MoS_2/WS_2,[7] $MoSe_2$/WSe_2,[8] WSe_2/MoS_2,[9,10] *etc.*) have been demonstrated to form p–n junctions, which serve as the basis for these optoelectronic devices. The main function of these heterostructures is the ability to mediate optical transitions and charge transfer across the junction of two materials,[11–13] and thus, maintaining a large-area, clean, and high-quality interface is of great importance. Unfortunately, to date most reported 2D heterostructures have been fabricated through mechanical transfer methods or multi-step chemical vapor deposition. While the former are troublesome

[a] *School of Materials Science and Engineering, Center of Advanced Lubrication and Seal Materials, Northwestern Polytechnical University, Xi'an, Shaanxi, 10072, China*
[b] *Department of Materials Science and Engineering, Northwestern University, Evanston, Illinois 60208, USA*
[c] *Northwestern University Atomic and Nanoscale Characterization Experimental (NUANCE) Center, Northwestern University, Evanston, Illinois 60208, USA. E-mail: x-chen@northwestern.edu*
[d] *Department of Mechanical Engineering, Northwestern University, Evanston, Illinois 60208, USA*
[e] *International Institute for Nanotechnology (IIN), Northwestern University, Evanston, Illinois 60208, USA. E-mail: v-dravid@northwestern.edu*

† Electronic supplementary information (ESI) available: Experimental details; XRD characterization; and transfer of a CVD-grown MoS_2 monolayer onto Cu_xS nanocrystals. See DOI: 10.1039/c8mh00809d

due to the interfacial contamination commonly introduced *via* the polymer-based transfer process, the latter is problematic due to challenges related to the lack of spatial control over the synthesized products, more limited heterojunction interface, and lack of consistent yields.[7]

Toward this end, exploring new geometries of TMD heterostructures beyond the existing library of 2D materials is of great interest for interface engineering and scalable production. Recently, surface decoration of TMD monolayers with nanocrystals[14–16] or quantum dots[17,18] of other chalcogenides has been studied as a typical approach to create heterojunctions. The resultant nanocomposites can effectively overcome the low optical cross-section of MoS_2 and thus lead to enhanced absorption[14] and improved photodetectivity.[18] For instance, chalcocite copper sulfide (Cu_xS) nanocrystals are one of the most interesting materials due to their natural abundance, p-type semiconductor nature, and relatively small band gap leading to strong light absorption from the visible to near infrared region.[19,20] When combined with MoS_2, the resultant band alignment at the interfaces can potentially enable superior interfacial charge transfer.[21,22] However, the reported preparation of the TMD heterostructures mostly relies on mechanical transfer[14,15] or solution-based chemical synthesis[16,17] and thus has been difficult to realize an uncontaminated and atomically-contacted sharp interface.

Herein, we introduce a new geometry design for the family of TMD heterostructures by encapsulating Cu_xS ($1.8 < x < 2$) nanocrystals with cap-like MoS_2 layered structures, namely Cu_xS@MoS_2 heterostructures. An atomically clean interface between the Cu_xS core and MoS_2 cap is created *via* direct chemical vapor deposition, which effectively maximizes the interfacial area and thus facilitates photoemission and charge transfer between the two materials. Using discrete dipole approximation (DDA), we examined the optical properties of these heterostructures, and density functional theory (DFT) calculations were carried out to better understand the band alignment and charge transfer dynamics at the heterojunction interface. The viability of these heterostructures for photodetection applications was evaluated as well. The results indicate that our Cu_xS@MoS_2 heterostructures exhibit highly improved light–matter interactions over a broad wavelength range compared to bare MoS_2, and thus lead to a strong photoresponse from violet to near-infrared light.

2. Results and discussion

The synthesis of Cu_xS@MoS_2 heterostructures is illustrated in Fig. 1a. Briefly, a 4 nm Cu film was first deposited on a Si/SiO_2 substrate by thermal evaporation and then annealed at 600 °C

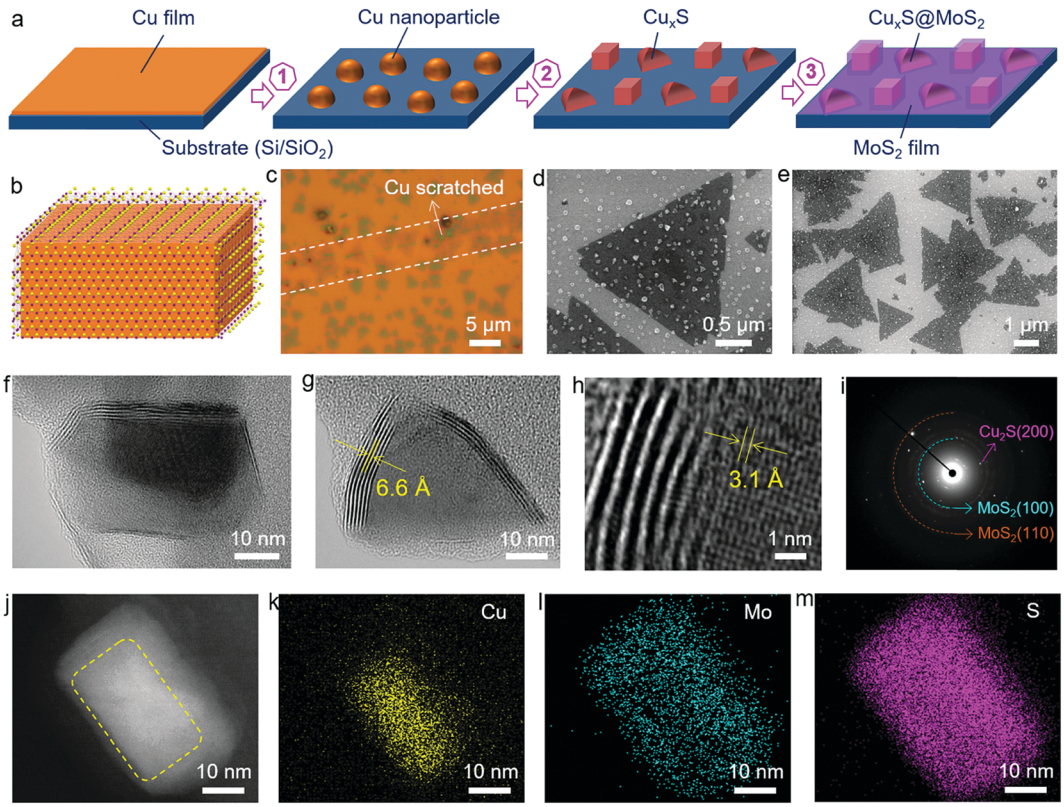

Fig. 1 Synthesis of Cu_xS@MoS_2 heterostructures. (a) Schematic illustrating the synthesis steps, including (1) annealing, (2) sulfurization, and (3) CVD. (b) Schematic of a single Cu_xS@MoS_2 heterostructure, illustrating the cap-like MoS_2 layers encapsulating a Cu_xS nanocrystal. (c) Optical view and (d and e) SEM images of the product after CVD. The substrate was left unexposed to the copper film in the dotted line region in (c). (f and g) TEM images of individual Cu_xS@MoS_2 heterostructures. (h) High-resolution TEM image indicating the atomic contact at the Cu_xS–MoS_2 interface and (i) the resultant diffraction pattern. (j) STEM image of a single heterostructure and (k–m) the corresponding EDS maps.

in a N_2 environment (step 1). The samples were then sulfurized at 600 °C (step 2) for 30 min. The encapsulation of MoS_2 caps was finally accomplished *via* a chemical vapor deposition process utilizing MoO_3 and S powders as precursors (step 3). The resultant product, Cu_xS@MoS_2 heterostructures, is schematically illustrated in Fig. 1b. An optical image of the resultant sample surface is shown in Fig. 1c. The Cu film within the dotted lines was removed by scratching prior to MoS_2 deposition. Thus, in this region, which exhibits a lighter optical contrast, we observed the growth of MoS_2 monolayers with no Cu_xS. The flakes outside the dotted region exhibit a relatively darker color due to the formation of Cu_xS@MoS_2 heterostructures, as indicated by the SEM images in Fig. 1d and e. One can also observe that the Cu_xS@MoS_2 nanocrystals are distributed uniformly throughout the substrate. It is worth noting that the size and distribution of the nanocrystals can be effectively modulated by varying the thickness of the preliminary Cu film and the ramp rate of the subsequent annealing process, similar to that we have otherwise demonstrated previously.[23] XRD patterns obtained over the entire substrate (Fig. S1, ESI†) indicate that the Cu_xS nanocrystals have a chalcocite structure with x varying from 1.8 to 2.0.

The TEM images in Fig. 1f and g confirm that the MoS_2 layers, with a layer-to-layer spacing of 6.6 Å and thickness of ~3–5 nm, cap the faceted Cu_xS nanocrystals. The high-resolution image (Fig. 1h) further indicates the direct atomic connection of Cu_xS and MoS_2 at the interface. Cu_xS exhibits a lattice spacing of 3.1 Å, corresponding to the (200) plane, which is also found to be the dominant facet of Cu_xS from the diffraction pattern (Fig. 1i). EDS maps obtained for a typical Cu_xS@MoS_2 heterostructure (Fig. 1j) demonstrate the elemental composition of Cu, Mo and S (Fig. 1k–m). The distribution of Cu is mostly concentrated inside the heterostructure as outlined in Fig. 1j, indicating effective MoS_2 encapsulation of the Cu_xS nanocrystals.

XPS spectra are further displayed in Fig. 2a–c. The spectra for the Cu_xS@MoS_2 heterostructures are compared to a control sample prepared by transferring a pre-grown MoS_2 monolayer onto Cu_xS nanocrystals (represented as Cu_xS/MoS_2 hereafter). Details about the MoS_2 transfer can be found in Fig. S2 (ESI†). The Mo and S spectra are generally consistent for both samples. The Mo 3d peaks at 233.11 eV and 229.92 eV correspond to the $3d_{5/2}$ and $3d_{3/2}$ doublets (Fig. 2a), while the S 2p peak can be deconvoluted into two peaks at 163.91 eV and 162.73 eV (Fig. 2b), which can be assigned to the $2p_{1/2}$ and $2p_{3/2}$ orbitals, respectively.[24,25] The peaks for metallic Mo or MoO_x are insignificant, suggesting high quality MoS_2 layers on both products. The Cu_xS@MoS_2 heterostructures present Cu 2p peaks at 952.32 eV ($2p_{1/2}$) and 932.45 eV ($2p_{3/2}$), which are consistent with the peak location of copper sulfides.[26] However, the intensities of the Cu peaks are weaker compared with the Mo and S peaks, due to the encapsulation of the MoS_2 layers. It is worth noting that peaks representing $CuSO_4$ are also observed on the transferred samples, probably due to the inevitable surface oxidation of Cu_xS in air, which indicates that MoS_2 encapsulation leads to improved air stability of the nanocrystals and serves as an additional highlight of this geometry.

Raman spectroscopy is used to assess the crystallinity and layer thickness of the MoS_2 layers through the two characteristic MoS_2 vibrational modes, E^1_{2g} and A_{1g}.[25,27] The E^1_{2g} mode is attributed to the in-plane vibration of Mo and S atoms, while the A_{1g} mode is related to the out-of-plane vibration of S atoms.[27] Fig. 2d shows the Raman spectra of monolayer MoS_2 (spectrum 1, obtained inside the dotted lines in Fig. 1b), Cu_xS/MoS_2 (spectrum 2) and Cu_xS@MoS_2 (spectrum 3). The Cu_xS@MoS_2 heterostructures exhibit two vibrational modes centered at 381.10 cm^{-1} and

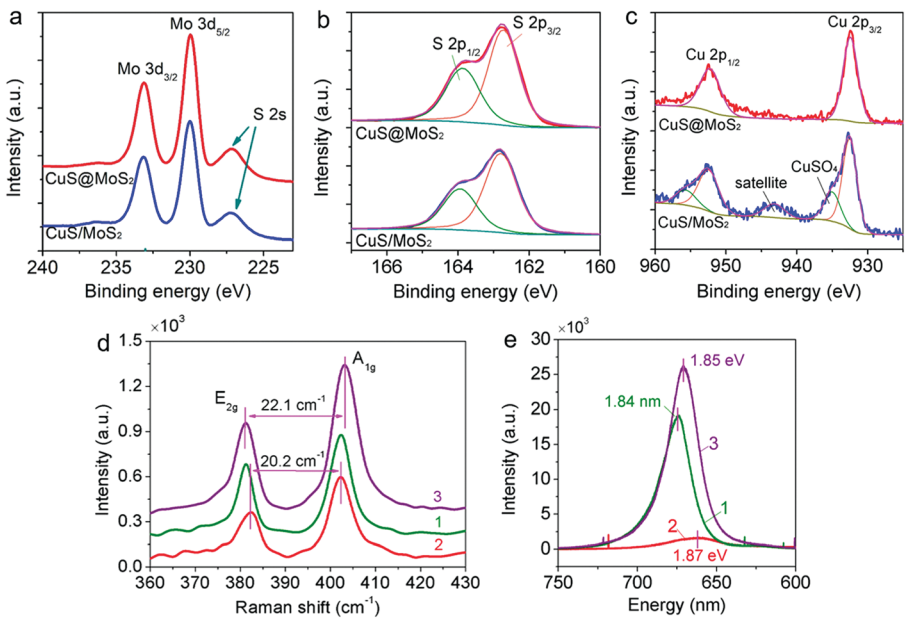

Fig. 2 Spectroscopic characterization. (a–c) XPS spectra of (a) Mo 3d, (b) S 2p and (c) Cu 2p for the Cu_xS@MoS_2 heterostructures and conventional MoS_2 monolayer transferred onto Cu_xS nanocrystals. (d) Raman and (e) photoluminescence spectra of (1) monolayer MoS_2 inside the dotted lines in Fig. 1c, (2) conventional MoS_2 monolayer transferred onto Cu_xS nanocrystals and (3) Cu_xS@MoS_2 heterostructures.

403.23 cm^{-1} with a E^1_{2g}-to-A_{1g} frequency difference of ~22.13 cm^{-1}. This value is smaller than that of bulk MoS_2, but larger than that of the pristine and transferred monolayer MoS_2, probably due to the multilayer nature of the MoS_2 caps.[28] The corresponding photoluminescence spectra are also collected at ambient temperature with a small laser power of 1 μW to avoid heating the sample. As shown in Fig. 2e, the pristine MoS_2 exhibits photoluminescence emission near ~674 nm and another insignificant emission peak around ~623 nm. The former is attributed to the A exciton emission due to the interband transition at the Brillouin zone *K* point in MoS_2, while the latter arises from the higher energy B exciton emission from another direct transition between the conduction band and a lower-lying valence band.[29,30] The Cu_xS@MoS_2 heterostructures exhibit equivalent photoluminescence emission peaks, with a slight blue-shift (670 nm) probably originating from the change in local strain because of the presence of Cu_xS cores.[31] It is worth noting that a remarkable quenching effect and more significant blue-shift (to 663 nm) of the photoluminescence were observed for the transferred MoS_2 sample, probably due to the inevitable contamination and released local strain from the original SiO_2 substrate after the transfer process.[32] This again proves the necessity of building a clean interface as demonstrated in our heterostructures.

The optical properties of the Cu_xS@MoS_2 heterostructures are further understood using the discrete dipole approximation (DDA) method. The simulation was carried out for a 50 × 25 × 25 nm^3 rectangular Cu_xS target and the same Cu_xS capped with 6-layer MoS_2 as shown in Fig. 3a and b, respectively. The details regarding the DDA method can be found in the Experimental section (ESI†).[33,34] The simulated absorption spectra are shown in Fig. 3c. The Cu_xS nanocrystal shows high absorption in the visible region (400 nm to 600 nm) as well as in the near infrared region (700 nm to 1000 nm), which is consistent with a previous experimental report.[35] The Cu_xS@MoS_2 heterostructure exhibits overall increased absorption in the visible region, with the emergence of two peaks at 673.1 nm and at 628.0 nm due to the presence of A and B exciton absorption pathways indicated in Fig. 3e.

The DDA calculations also model the interaction of the refractive index with the geometry and incident light to evaluate the electric field distribution,[33] which is an indicator of the magnitude of the light–matter interaction present. Fig. 3d–i display the front view (arrow direction in Fig. 3a) of the obtained electric field maps of both targets at different incident wavelengths (400 nm, 610 nm and 900 nm). The electric field strength ($|E/E_0|^2$) can be correlated with the absorption efficiency at various locations of the sample in Fig. 3c. Overall, one can observe that the Cu_xS nanocrystal shows a weak electric field response (Fig. 3d–f), while the electric field distribution of the Cu_xS@MoS_2 heterostructure is confined to the MoS_2 cap, with significantly enhanced strength (Fig. 3g–i), suggesting the significant improvement of the light–matter interactions due to the formation of a heterojunction. This aspect is particularly clear under an incident radiation of 900 nm, where even though coupling of light with the localized surface plasmon resonance (LSPR) of Cu_xS leads to an enhanced electric field in the bare nanocrystal.[36,37]

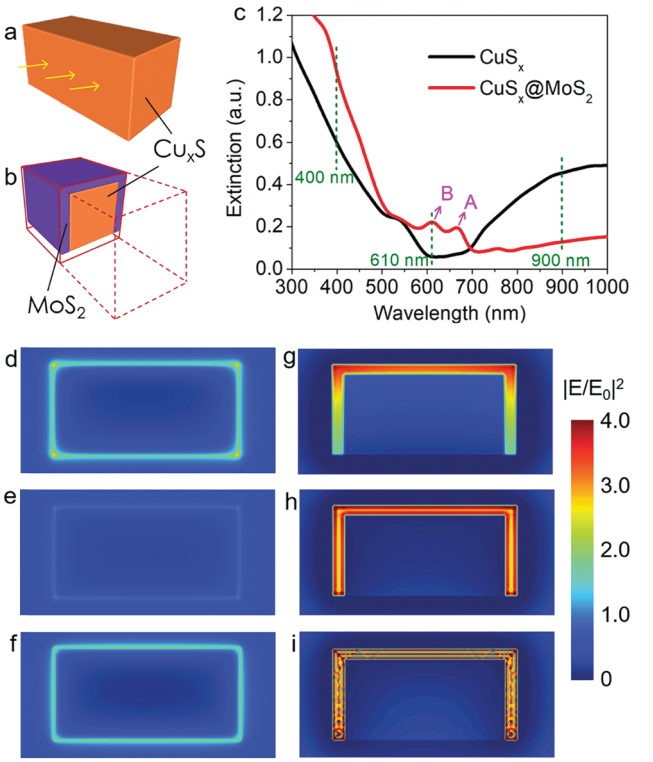

Fig. 3 Simulation of light–matter interactions. (a and b) 3D models for the Cu_xS (a) and Cu_xS@MoS_2 (b) targets used for DDA modeling. The arrows indicate the direction of incident light applied for all simulated targets unless otherwise noted. (c) Calculated extinction (absorption + scattering) efficiency as a function of incident wavelength. The A and B labels correspond to the A and B excitons observed in the photoluminescence spectra (Fig. 2e). (d–i) Calculated electric field distributions on Cu_xS (d–f) and Cu_xS@MoS_2 (g–i) nanocrystals under various incident wavelengths: (d and g) 400 nm, (e and h) 610 nm, and (f and i) 900 nm.

By contrast, the Cu_xS@MoS_2 heterostructure exhibits a stronger response, due to the possible plasmonic coupling enabled by the clean Cu_xS–MoS_2 interface.[31] These simulations suggest that our Cu_xS@MoS_2 heterostructure is a promising optoelectronic material particularly for applications where a near infrared source is required.

The DDA results theoretically suggest interesting light–matter interactions in our Cu_xS@MoS_2 heterostructures, allowing us to further explore their potential application in broadband optoelectronics. A field-effect phototransistor made from the Cu_xS@MoS_2 heterostructures was constructed with the schematic provided in Fig. 4a. In this device geometry, Cu_xS@MoS_2 heterostructures act as the light sensitizers, while the underlying MoS_2 monolayers act as the channel material (Fig. 4b). A similar transistor made from the transferred Cu_xS/MoS_2 is also studied for comparison. All measurements were carried out at room temperature. As shown in Fig. 4c, the transferred Cu_xS/MoS_2 device exhibits a typical n-type channel behavior, which is consistent with the n-type nature of monolayer MoS_2.[30] The Cu_xS@MoS_2 device also shows an n-type electronic behavior; however, a gate-dependent drain current was only observed for small positive gate voltages before immediately saturating.

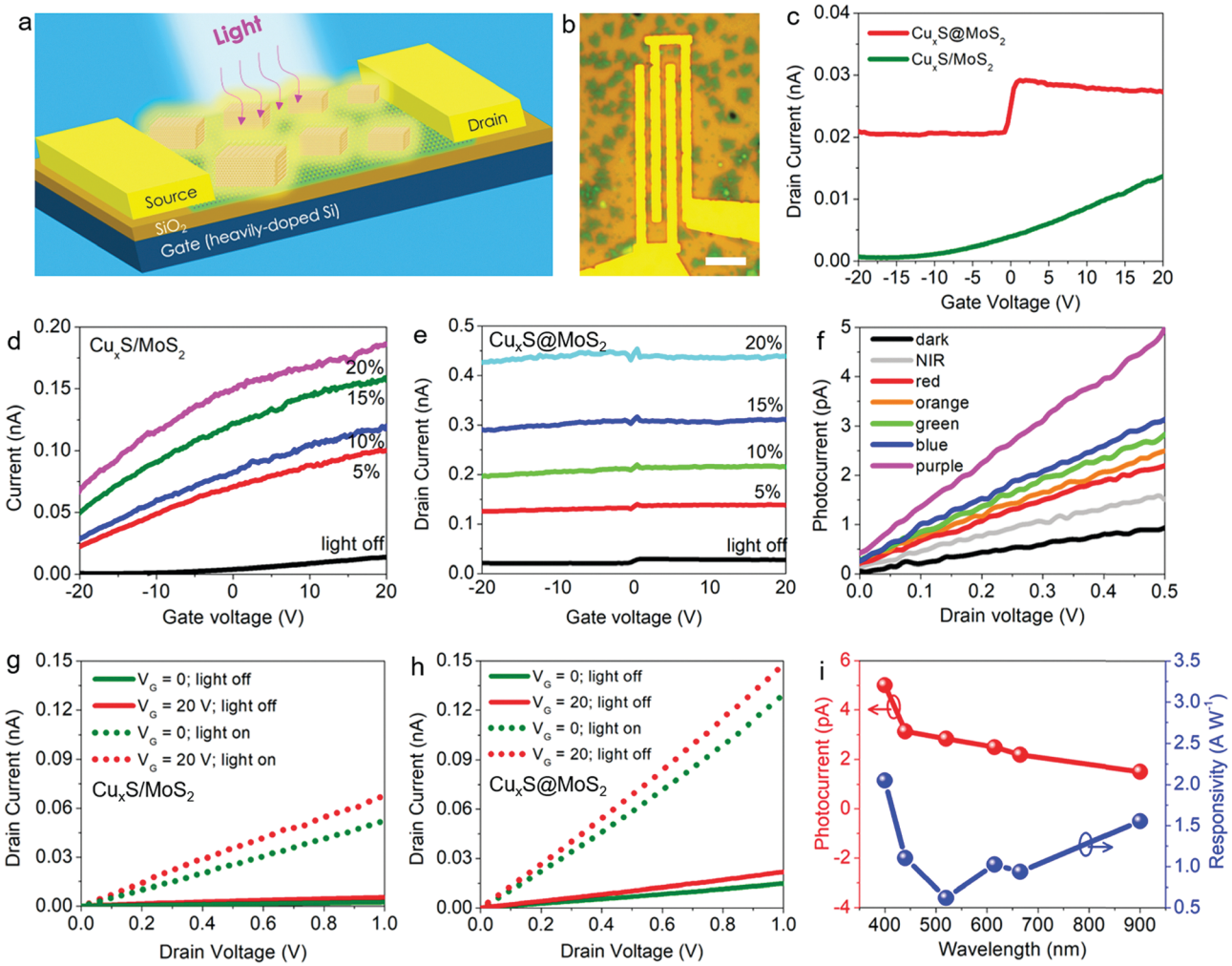

Fig. 4 Optoelectronic device application. (a) Device design and (b) optical view of the phototransistor. Scale bar in (b): 5 μm. (c) Transfer characteristics of the Cu_xS/MoS_2 and $Cu_xS@MoS_2$ devices. (d and e) Transfer curves of Cu_xS/MoS_2 (d) and $Cu_xS@MoS_2$ (e) transistors under illumination with varying power. (f and g) Output curves of Cu_xS/MoS_2 (f) and $Cu_xS@MoS_2$ (g) transistors with and without illumination. (h) Output curve of the $Cu_xS@MoS_2$ device with illuminations of different wavelengths. (i) Photocurrent and photoresponsivity of the $Cu_xS@MoS_2$ device as a function of illumination wavelength.

This is possibly due to the Fermi level of MoS_2 being aligned with that of p-type Cu_xS after the formation of the heterojunction. A further increase of the gate voltage in the positive direction can lead to misalignment in these bands, which would induce a decrease in the current.[38] From the transfer curves, we obtain a carrier mobility of 1.76×10^{-4} cm^2 V^{-1} s^{-1} for the $Cu_xS@MoS_2$ device and 0.11×10^{-4} cm^2 V^{-1} s^{-1} for the Cu_xS/MoS_2 device. It is also worth noting that both devices show a relatively weak gate dependence with ON/OFF ratios of 1.2–1.5,[39] which is probably due to the electric field screening provided by the underlying Cu_xS nanocrystals. The dependence of transfer curves on the illumination power for the Cu_xS/MoS_2 and $Cu_xS@MoS_2$ transistors is demonstrated in Fig. 4d and e, respectively. Both devices show a photocurrent generation ability over the entire gate voltage range, which is also consistent with the results previously reported for monolayer MoS_2 transistors.[40] However, the photoresponse of the $Cu_xS@MoS_2$ device is more significant, with a negligible gate dependence, and exhibits a linear relationship with the increase of illumination power, which is usually more desirable for practical optoelectronics.

The output curves in the dark and light states for both devices are further shown in Fig. 4f and g. It is worth mentioning that the linear relationship between the drain current and drain voltage indicates good ohmic contact of the channel materials and contact electrodes. One can again observe that the $Cu_xS@MoS_2$ device exhibits a more substantial photoresponse compared to the Cu_xS/MoS_2 device. The output curves of the $Cu_xS@MoS_2$ device at various illumination wavelengths are shown in Fig. 4h. The device shows remarkable response for wavelengths ranging from the violet to near infrared region due to the presence of small-band gap Cu_xS, which is one of the key advantages of the heterostructure compared to MoS_2 devices. The corresponding photocurrent and the calculated photoresponsivity are further displayed in Fig. 4i. The trend of photoresponsivity variation according to the incident wavelength is consistent with the absorption curve of $Cu_xS@MoS_2$ in Fig. 3c. It is worth noting that the photoresponsivity under near infrared

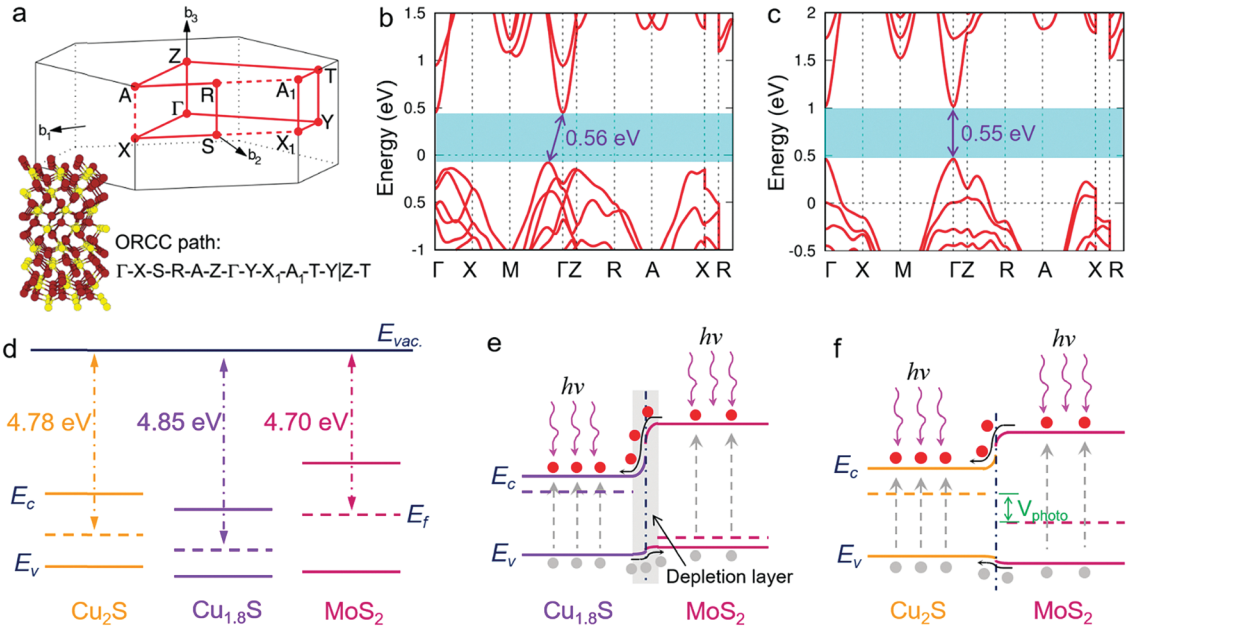

Fig. 5 Electronic structure calculations. (a) High symmetry points in the Brillouin zone of Cu_xS. The inset shows the corresponding atomic structure. (b and c) Band structures calculated for Cu_2S (b) and $Cu_{1.8}S$ (c). (d) Calculated energy band diagram for Cu_2S, $Cu_{1.8}S$, and MoS_2. (e and f) Schematics showing the possible formation of a type-II heterojunction between $Cu_{1.8}S$ and MoS_2 (e) and a type-I heterojunction between Cu_2S and MoS_2 (f) under illumination.

incident radiation is significantly pronounced compared to the absorption spectra (consistent with the near field distribution in Fig. 3i). This should be enabled by (1) the band bending and electric fields present at the heterojunction interface between MoS_2 and a small-band gap material and (2) possibly the strong light–matter interaction due to the LSPR effect as theoretically predicted in Fig. 3i and experimentally demonstrated in our previous report,[41] further suggesting the potential of our TMD heterostructures in broadband optoelectronics.

Finally, we performed density functional theory (DFT) calculations to understand and corroborate our experimental findings and conclusions regarding the optoelectronic properties of this heterostructure. Fig. 5a shows high symmetry points in the Brillouin zone of Cu_xS (inset atomic structure) used for the calculation. The obtained electronic band structures for Cu_2S and $Cu_{1.8}S$ are shown in Fig. 5b and c, respectively. We find that the ideal chalcocite Cu_2S has an indirect band gap of 0.56 eV; however, the band structure can be effectively modulated by introducing Cu vacancies in the system. For instance, the chalcocite $Cu_{1.8}S$ is found to exhibit a direct band gap of 0.55 eV (Fig. 5c). This suggests that the incorporation of Cu_xS can not only supplement the low IR absorption for MoS_2 (Fig. 3c), but also significantly improve the photoelectronic effect since the photon-related excitation and emission in the slightly deficient Cu_xS are significantly improved.

The DFT calculations also reveal the work function of the components, which allows us to predict the alignment of the band structure at the interface. Fig. 5d shows the band energy diagram of the Cu_2S, $Cu_{1.8}S$ and MoS_2 systems before heterojunction formation. Again, this directly indicates the modulation of the band structure of Cu_xS with slight variations in the stoichiometry (see more details in Fig. S3, ESI†), and accordingly we are able to predict possible charge transfer pathways following heterojunction formation. As shown in Fig. 5e and f, Cu_xS–MoS_2 is expected to exhibit better photocarrier separation efficiency due to the formation of a type-II band alignment (Fig. 5e), as compared with the possible type-I heterojunction formed in the Cu_2S–MoS_2 system (Fig. 5f). Thus, combined with evidence from our optical results, we can surmise that the noteworthy optoelectronic performance of our Cu_xS@MoS_2 phototransistor is probably attributed to a comprehensive contribution from (1) the improved interfacial charge transfer that originated from the clean, atomically-connected interface, (2) the formation of a type-II heterojunction structure between Cu_xS and MoS_2, and (3) the potentially enhanced light–matter interactions due to the LSPR of Cu_xS.

3. Conclusions

In summary, we explored a new route for the geometry design and synthesis of TMD heterostructures beyond traditional lateral/vertical heterostructures. The heterojunction formation was accomplished *via* a single-step direct chemical vapor deposition of MoS_2 on nanocrystals of another transition metal sulfide. The resultant product, *e.g.*, Cu_xS@MoS_2 heterostructures, has an appreciable atomically-sharp interface area and is found to exhibit strongly improved light–matter interactions over a broad wavelength range. The formation of this heterojunction also leads to useful band alignment and can potentially facilitate the charge separation and transfer in an optoelectronic process. The field-effect phototransistor based on the Cu_xS@MoS_2 heterostructures represents interesting transfer characteristics, and

importantly, a constant photoresponse is observed throughout the entire positive and negative gate voltage regions. The photocurrent generation was observed over a broadband range, particularly for the near infrared photodetection enabled by the band alignment at the heterojunction as well as the surface plasmon effect from Cu_xS. As such, this geometry potentially serves as a new scalable material system for future optoelectronic semiconductor devices.

Conflicts of interest

There are no conflicts to declare.

Acknowledgements

This material is based on the work supported by the National Science Foundation (NSF) under Grant No. DMR-1507810. This work made use of the EPIC, Keck-II, and SPID facilities of Northwestern University's NU*ANCE* Center, which received support from the Soft and Hybrid Nanotechnology Experimental (SHyNE) Resource (NSF ECCS-1542205); the MRSEC program (NSF DMR-1720139) at the Materials Research Center; the International Institute for Nanotechnology (IIN); the Keck Foundation; and the State of Illinois, through the IIN. J. G. D. gratefully acknowledges support from the National Science Foundation Graduate Research Fellowship Program (NSF-GRFP). A. A. M. gratefully acknowledges support from the Ryan Fellowship and the International Institute for Nanotechnology at Northwestern University.

References

1 Q. H. Wang, K. Kalantar-Zadeh, A. Kis, J. N. Coleman and M. S. Strano, Electronics and Optoelectronics of Two-Dimensional Transition Metal Dichalcogenides, *Nat. Nanotechnol.*, 2012, **7**, 699.
2 M. Chhowalla, D. Jena and H. Zhang, Two-dimensional semiconductors for transistors, *Nat. Rev. Mater.*, 2016, **1**, 16052.
3 C. Tan, Z. Liu, W. Huang and H. Zhang, Non-volatile resistive memory devices based on solution-processed ultrathin two-dimensional nanomaterials, *Chem. Soc. Rev.*, 2015, **44**, 2615.
4 H. Zhang, Ultrathin two-dimensional nanomaterials, *ACS Nano*, 2015, **9**, 9451.
5 X. Zhang, Z. Lai, Q. Ma and H. Zhang, Novel structured transition metal dichalcogenide nanosheets, *Chem. Soc. Rev.*, 2018, **47**, 3301.
6 C. Tan, X. Cao, X. Wu, Q. He, J. Yang, X. Zhang, J. Chen, W. Zhao, S. Han, G. H. Nam, M. Sindoro and H. Zhang, Recent advances in ultrathin two-dimensional nanomaterials, *Chem. Rev.*, 2017, **117**, 6225.
7 Y. Gong, J. Lin, X. Wang, G. Shi, S. Lei, Z. Lin and H. Terrones, Vertical and in-plane heterostructures from WS_2/MoS_2 monolayers, *Nat. Mater.*, 2014, **13**, 1135.
8 C. Huang, S. Wu, A. M. Sanchez, J. J. Peters, R. Beanland, J. S. Ross and X. Xu, Lateral heterojunctions within monolayer $MoSe_2$–WSe_2 semiconductors, *Nat. Mater.*, 2014, **13**, 1096.
9 M. Y. Li, Y. Shi, C. C. Cheng, L. S. Lu, Y. C. Lin, H. L. Tang and W. H. Chang, Epitaxial growth of a monolayer WSe_2–MoS_2 lateral pn junction with an atomically sharp interface, *Science*, 2015, **349**, 524.
10 X. Duan, C. Wang, J. C. Shaw, R. Cheng, Y. Chen, H. Li and J. Jiang, Lateral epitaxial growth of two-dimensional layered semiconductor heterojunctions, *Nat. Nanotechnol.*, 2014, **9**, 1024.
11 F. Ceballos, M. Z. Bellus, H. Y. Chiu and H. Zhao, Ultrafast charge separation and indirect exciton formation in a MoS_2–$MoSe_2$ van der Waals heterostructure, *ACS Nano*, 2014, **8**, 12717.
12 H. Chen, X. Wen, J. Zhang, T. Wu, Y. Gong, X. Zhang and W. Zhuang, Ultrafast formation of interlayer hot excitons in atomically thin MoS_2/WS_2 heterostructures, *Nat. Commun.*, 2016, **7**, 12512.
13 D. Kozawa, A. Carvalho, I. Verzhbitskiy, F. Giustiniano, Y. Miyauchi, S. Mouri and G. Eda, Evidence for fast interlayer energy transfer in $MoSe_2/WS_2$ heterostructures, *Nano Lett.*, 2016, **16**, 4087.
14 X. Sun, H. Deng, W. Zhu, Z. Yu, C. Wu and Y. Xie, Interface Engineering in Two-Dimensional Heterostructures: Towards an Advanced Catalyst for Ullmann Couplings, *Angew. Chem., Int. Ed.*, 2016, **55**, 1704.
15 Y. Wen, L. Yin, P. He, Z. Wang, X. Zhang, Q. Wang and F. Wang, Integrated high-performance infrared phototransistor arrays composed of nonlayered PbS–MoS_2 heterostructures with edge contacts, *Nano Lett.*, 2016, **16**, 6437.
16 P. Sahatiya, A. Kadu, H. Gupta, P. Thanga Gomathi and S. Badhulika, Flexible disposable cellulose paper based MoS_2–Cu_2S hybrid for wireless environmental monitoring and multifunctional sensing of chemical stimuli, *ACS Appl. Mater. Interfaces*, 2018, **10**, 9048.
17 J. Schornbaum, B. Winter, S. P. Schießl, F. Gannott, G. Katsukis, D. M. Guldi and J. Zaumseil, Epitaxial Growth of PbSe Quantum Dots on MoS_2 Nanosheets and their Near-Infrared Photoresponse, *Adv. Funct. Mater.*, 2014, **24**, 5798.
18 D. Kufer, I. Nikitskiy, T. Lasanta, G. Navickaite, F. H. Koppens and G. Konstantatos, Hybrid 2D–0D MoS_2–PbS quantum dot photodetectors, *Adv. Mater.*, 2015, **27**, 176.
19 A. B. Wong, S. Brittman, Y. Yu, N. P. Dasgupta and P. Yang, Core–shell CdS–Cu_2S nanorod array solar cells, *Nano Lett.*, 2015, **15**, 4096.
20 A. B. Martinson, S. C. Riha, E. Thimsen, J. W. Elam and M. J. Pellin, Structural, optical, and electronic stability of copper sulfide thin films grown by atomic layer deposition, *Energy Environ. Sci.*, 2013, **6**, 1868.
21 Y. Wang, H. Li, Y. Zhang, Y. Peng, P. Zhang and J. Zhao, Self-templating thermolysis synthesis of $Cu_{2-x}S$@M (M = C, TiO_2, MoS_2) hollow spheres and their application in rechargeable lithium batteries, *Nano Res.*, 2018, **11**, 831.
22 C. Pan, S. Niu, Y. Ding, L. Dong, R. Yu, Y. Liu and Z. L. Wang, Enhanced Cu_2S/CdS coaxial nanowire solar cells by piezo-phototronic effect, *Nano Lett.*, 2012, **12**, 3302.
23 Y. Li, K. Burnham, J. Dykes and N. Chopra, Self-patterning of graphene-encapsulated gold nanoparticles for surface-enhanced Raman spectroscopy, *MRS Commun.*, 2018, **8**, 79.

24 K. M. McCreary, A. T. Hanbicki, J. T. Robinson, E. Cobas, J. C. Culbertson, A. L. Friedman and B. T. Jonker, *Adv. Funct. Mater.*, 2014, **24**, 6449.
25 A. S. George, Z. Mutlu, R. Ionescu, R. J. Wu, J. S. Jeong, H. H. Bay and C. S. Ozkan, *Adv. Funct. Mater.*, 2014, **24**, 7461.
26 M. C. Biesinger, B. R. Hart, R. Polack, B. A. Kobe and R. S. C. Smart, Analysis of mineral surface chemistry in flotation separation using imaging XPS, *Miner. Eng.*, 2007, **20**, 152.
27 S. Wang, X. Wang and J. H. Warner, All Chemical Vapor Deposition Growth of MoS_2: h-BN Vertical van der Waals Heterostructures, *ACS Nano*, 2015, **9**, 5246.
28 H. Li, Q. Zhang, C. C. R. Yap, B. K. Tay, T. H. T. Edwin, A. Olivier and D. Baillargeat, From bulk to monolayer MoS_2: evolution of Raman scattering, *Adv. Funct. Mater.*, 2012, **22**, 1385.
29 G. Eda, H. Yamaguchi, D. Voiry, T. Fujita, M. Chen and M. Chhowalla, Photoluminescence from chemically exfoliated MoS_2, *Nano Lett.*, 2011, **11**, 5111.
30 W. Choi, M. Y. Cho, A. Konar, J. H. Lee, G. B. Cha, S. C. Hong and S. Kim, High-Detectivity Multilayer MoS_2 Phototransistors with Spectral Response from Ultraviolet to Infrared, *Adv. Mater.*, 2012, **24**, 5832.
31 Y. Li, J. D. Cain, E. D. Hanson, A. A. Murthy, S. Hao, F. Shi, Q. Li, C. Wolverton, X. Chen and V. P. Dravid, Au@ MoS_2 core–shell heterostructures with strong light–matter interactions, *Nano Lett.*, 2016, **16**, 7696.
32 W. H. Chae, J. D. Cain, E. D. Hanson, A. A. Murthy and V. P. Dravid, Substrate-induced strain and charge doping in CVD-grown monolayer MoS_2, *Appl. Phys. Lett.*, 2017, **111**, 143106.
33 B. T. Draine and P. J. Flatau, User guide for the discrete dipole approximation code DDSCAT 7.3, 2013, arXiv preprint arXiv, 1305.6497.
34 Y. Li, W. Shi and N. Chopra, Functionalization of multilayer carbon shell-encapsulated gold nanoparticles for surface-enhanced Raman scattering sensing and DNA immobilization, *Carbon*, 2016, **100**, 165.
35 A. C. Poulose, S. Veeranarayanan, M. S. Mohamed, Y. Nagaoka, R. R. Aburto, T. Mitcham and T. Maekawa, Multi-stimuli responsive Cu_2S nanocrystals as trimodal imaging and synergistic chemo-photothermal therapy agents, *Nanoscale*, 2015, **7**, 8378.
36 J. M. Luther, P. K. Jain, T. Ewers and A. P. Alivisatos, Localized surface plasmon resonances arising from free carriers in doped quantum dots, *Nat. Mater.*, 2011, **10**, 361.
37 Y. Xie, A. Riedinger, M. Prato, A. Casu, A. Genovese, P. Guardia, S. Sottini, C. Sangregorio, K. Miszta and S. Ghosh, Copper Sulfide Nanocrystals with Tunable Composition by Reduction of Covellite Nanocrystals with Cu^+ ions, *J. Am. Chem. Soc.*, 2013, **135**, 17630.
38 D. Jariwala, V. K. Sangwan, C. C. Wu, P. L. Prabhumirashi, M. L. Geier, T. J. Marks and M. C. Hersam, Gate-Tunable Carbon Nanotube–MoS_2 Heterojunction pn Diode, *Proc. Natl. Acad. Sci. U. S. A.*, 2013, **110**, 18076.
39 Z. Yin, H. Li, H. Li, L. Jiang, Y. Shi, Y. Sun and H. Zhang, Single-layer MoS_2 phototransistors, *ACS Nano*, 2011, **6**, 74.
40 O. Lopez-Sanchez, D. Lembke, M. Kayci, A. Radenovic and A. Kis, Ultrasensitive photodetectors based on monolayer MoS_2, *Nat. Nanotechnol.*, 2013, **8**, 497.
41 Y. Li, J. G. DiStefano, A. A. Murthy, J. D. Cain, E. D. Hanson, Q. Li, F. C. Castro, X. Chen and V. P. Dravid, Superior Plasmonic Photodetectors Based on Au@ MoS_2 Core–Shell Heterostructures, *ACS Nano*, 2017, **11**, 10321.

